




Cite this: DOI: 10.1039/d5nj02838h

Lanthanide coordination in *N*-acyl diphenylalanine organohydrogels

Tsuimy Shao,^{ab} Mozhgan Khorasani Motlagh,^b Meissam Noroozifar^b and Heinz-Bernhard Kraatz  ^{*ab}

Three different *N*-acylated diphenylalanine peptide conjugates with varying lengths of fatty acid tails were synthesized and characterized through ¹H NMR, FT-IR, MS, and elemental analysis. The organo-hydrogelation of these peptides was studied using two organic solvents, DMF and DMSO, as well as in the presence of Tb³⁺, which resulted in successful gelation for three previously non-gelling conditions. The viscoelastic properties of these gels were also investigated through rheological frequency sweeps. The morphologies of the organo-hydrogel hybrids were also examined through TEM and SEM. Through mass spectrometry, we demonstrate a variety of Tb³⁺–peptide–solvent coordinated species owing to the variable geometries characteristic of lanthanides and the self-assembling nature of physical gels, driven by noncovalent interactions. A 1:1 peptide:Tb³⁺ ratio was found to yield the highest fluorescence intensity at 546 nm, though even 0.2 eq. of peptide enhanced the innate fluorescent properties of Tb³⁺. Thus, through control of the peptide:Tb³⁺ ratio, a wide potential range of fluorescent gels with variable viscoelastic properties can be developed with tunable properties.

Received 12th July 2025,
Accepted 24th July 2025

DOI: 10.1039/d5nj02838h

rsc.li/njc

Introduction

Gels are a class of soft materials that have recently emerged as stimuli-responsive, functional, smart materials.¹ This has vastly expanded the scope of gel applications.¹ Gels can either be physical, formed through self-assembly *via* noncovalent interactions, or chemical, resulting from covalent crosslinking.^{1,2} Regardless, the gelators form three-dimensional networks that are capable of encapsulating large amounts of solvent, forming organogels from organic solvents or hydrogels from aqueous solutions.^{2,3} One of the key factors underlying the prevalence of gel development and applications is the flexibility of gel design. Starting with the gelator molecules, these can range from synthetic polymers^{4–6} to biopolymers^{7–9} to peptides.^{10–12} The ideal gelation conditions can vary depending on the gelator molecules, not only from organic or aqueous but also based on pH, salt concentrations, temperature, and even light.¹³ Additionally, gel formation by solvent encapsulation can concurrently result in the encapsulation of other molecules.¹⁴ Thus, there can be some unpredictability amongst these soft materials' properties, owing to gelator design, solvent composition, *etc.*, following the spontaneity of self-assembly that must be

studied for these soft materials to become tunable and functional for broad or targeted applications.

Metal ion incorporation into gels has long been studied and has produced a variety of materials with interesting applications.^{15,16} Among the less studied are lanthanide-containing biomaterials. Lanthanides, such as terbium and europium, have interesting coordination chemistry and geometries as well as fluorescence properties that have led to their intriguing applications.¹⁷ He *et al.*¹⁸ reported the use of a series of lanthanides (such as La³⁺, Eu³⁺, Tb³⁺) in the mediation of a collagen peptide self-assembly into photoluminescent helical nanoropes, although an aggregated biomaterial rather than a gel-based biomaterial. Chen *et al.*¹⁹ used Eu³⁺ in the preparation of a LAPONITE[®]-based organic/inorganic hybrid hydrogel, whose fluorescence and subsequent quenching with Cu²⁺ through photoinduced electron transfer (PET) allowed for applications in glutathione sensing and detection. The presence of glutathione disrupts PET by removing Cu²⁺, thereby restoring fluorescence. More recently, research on lanthanide-containing gel materials has focused on the functional properties that enable gels to flourish. Gu *et al.*²⁰ used a phenylbenzoic acid-based ligand for the formation of a Tb³⁺ metal–organic gel for the detection of organic amines. Li *et al.*²¹ reported a multistimuli-responsive bilayered hydrogel with Ln/2,6-pyridinedicarboxylic acid complexes with polymerizable sites (Ln–L₃) composed of chitosan–polyacrylamide–Eu–L₃ and poly-*n*-isopropyl-acrylamide–Tb–L₃. This bilanthanide bilayered material was reported as a hydrogel actuator that, under pH and heat stimulation, demonstrated shape memory and reversible luminescence switch behaviours.

^a Department of Chemistry, University of Toronto, 80 St. George Street, M5S 3H6, Toronto, Canada. E-mail: bernie.kraatz@utoronto.ca; Tel: +1-416-287-7197

^b Department of Physical and Environmental Sciences, University of Toronto Scarborough, 1065 Military Trail, M1C 1A4, Scarborough, Canada


Here, we report a series of *N*-acylated diphenylalanine (carbon tails of $n = 10, 14, 18$) organohydrogel hybrids containing Tb^{3+} . Previous work with diphenylalanine-based hydrogels has demonstrated the robustness of this motif in the encapsulation of a variety of biomolecules while preserving the gel's soft material properties.^{22,23} Zhou *et al.*²⁴ also demonstrated the ability of the phenylalanine motif to coordinate Tb^{3+} through the use of Fmoc-Phe in methanol/water. This amino acid-metal solution displayed responsive and reversible gelation in basic and acidic conditions, whereby the titration of NaOH and HCl triggered gel- and sol-state, respectively, along with an "on-off" luminescence effect. Many other lanthanide-containing gels, however, have been developed through polymerization, such as the previously stated acrylamide-based sample,²¹ or with more complex biomolecules, such as collagen¹⁸ or DNA.²⁵ With our low-molecular-weight simple peptide conjugate design, we demonstrate the effect of carbon chain length on the self-assembled morphologies in these Tb^{3+} -containing peptide gels through SEM imaging. We also show the variety of Tb^{3+} -peptide coordinated species present in the organohydrogel hybrid materials through mass spectroscopy, which are speculated to exist due to the physical nature of these gels being reliant on noncovalent-interaction-driven self-assembly. The range of species found supports the spontaneity of the self-assembly process to kinetically trap the lanthanide-coordinate peptides into metastable gels over thermodynamically stable, ordered, equilibrium states.

Experimental

Reagents

Boc-Phe-OH was purchased from MilliporeSigma (formerly Sigma Aldrich), Mississauga, ON, Canada. Phe-OMe was purchased from Advanced ChemTech, Louisville, KY, USA. Coupling reagents EDC·HCl (1-ethyl 3-(3'-dimethylaminopropyl)carbodiimide) and 6-Cl-HOBt (1-hydroxy-6-chloro-benzotriazole) were purchased from Matrix Innovations, QC, Canada. All other chemicals were purchased from MilliporeSigma (formerly Sigma Aldrich), Mississauga, ON, Canada. Chemicals were used without further purification. 18.2 MΩ cm Milli-Q water was used in all sample preparation.

Apparatus

^1H NMR spectra of the products were recorded on a Bruker 500 MHz NMR spectrometer (Bruker Co., Chemlingen, Germany) by dissolving in $\text{DMSO}-d_6$. An Agilent 6530 Accurate-Mass Q-TOF spectrometer was used for mass analysis. To probe the potential Tb-peptide coordinated species in the prepared gels, 1:1 Tb:peptide gels in DMF/ H_2O and $\text{DMSO}/\text{H}_2\text{O}$ were lyophilized and then dissolved in ethanol before MS characterization. Fourier transform-infrared (FT-IR) spectra of the samples were obtained using a Bruker Alpha FT-IR spectrometer equipped with a diamond for attenuated total reflection. A Flash 2000 CHN Analyzer was used for elemental analysis. The viscoelastic properties of the resulting self-assembled gels were studied with frequency sweep experiments using a Discovery Hybrid Rheometer-10 from TA Instruments with a 20 mm,

stainless steel sandblasted parallel plate geometry at 25 °C. Self-assembled nanostructures were examined through TEM, imaged with a Hitachi 7500 transmission electron microscope, and SEM, imaged with a Hitachi S530 scanning electron microscope. For TEM, samples were prepared on a copper TEM grid (300 mesh size), purchased from electron microscopy sciences, coated with a carbon film, and air dried for at least 24 hours before imaging. For SEM, hydrogels were lyophilized 24 hours before osmium coating for imaging. Emission spectra were obtained with a PTi Quantmaster 40 spectrofluorometer, with excitation at 260 nm and emission recorded from 450 to 700 nm. Peptides (2 mM) were dissolved in ethanol/water (1:1 v/v) in a 1 cm quartz cuvette. The fluorescence and coordination behaviour of Tb^{3+} with the peptides was monitored for 2 mM Tb^{3+} (1 eq.) with relative peptide ratios of 0.2, 0.4, 0.6, 0.8, 1.0, 2.0, 3.0, 4.0, and 5.0.

N-Acylated peptide conjugate synthesis

All fatty acid-peptide conjugates were synthesized following that of our previously reported myristylated diphenylalanine (C_{14} -FF-OH).^{22,23} Following the same synthesis leading to Boc-FF-OMe, Boc-deprotection of Boc-FF-OMe with TFA and neutralization with TEA under N_2 , the fatty acids capric and stearic acid (1 eq.) were coupled to Phe-Phe-OMe (1.6 eq.) with EDC/6-Cl-HOBt (2 eq.) in DCM with TEA. After standard aqueous workup (twice each with 10% w/v citric acid, saturated NaHCO_3 , and saturated NaCl) and column chromatography using a hexanes/ethyl acetate eluent system, the fatty acid-diphenylalanine methyl esters were hydrolyzed with NaOH (12.5 eq.) in water/1,4-dioxane (1:1 v/v). Final fatty acid-peptide conjugates, caprylated diphenylalanine (C_{10} -FF-OH; **1**), myristylated diphenylalanine (C_{14} -FF-OH; **2**), and stearylalated diphenylalanine (C_{18} -FF-OH; **3**), were collected after acidification, ethyl acetate extraction, and rotary evaporation/precipitation. ^1H NMR and MS results can be found in Fig. S1-S4.

C_{10} -FF-OH: ^1H NMR (500 MHz, DMSO) δ 12.77 (s, 1H), 8.22 (d, $J = 7.7$ Hz, 1H), 7.94 (d, $J = 8.7$ Hz, 1H), 7.31–7.12 (m, 10H), 4.54 (ddd, $J = 10.3, 8.6, 4.0$ Hz, 1H), 4.45 (td, $J = 8.2, 5.2$ Hz, 1H), 3.07 (dd, $J = 13.9, 5.2$ Hz, 1H), 3.01–2.90 (m, 2H), 2.67 (dd, $J = 13.9, 10.5$ Hz, 1H), 2.01–1.93 (m, 2H), 1.36–1.11 (m, 12H), 1.10–0.97 (m, 2H), 0.86 (t, $J = 6.9$ Hz, 3H). ESI-MS calcd m/z 466.2832 [$\text{C}_{28}\text{H}_{38}\text{N}_2\text{O}_4$] $^+$; found m/z 467.2914 [($\text{C}_{28}\text{H}_{38}\text{N}_2\text{O}_4$) + H] $^+$. Elemental analysis for $\text{C}_{28}\text{H}_{38}\text{N}_2\text{O}_4$ calcd: C 72.07%, H 8.21%, N 6.00%; found: C 72.11%, H 8.41%, N 5.82%.

C_{18} -FF-OH: ^1H NMR (500 MHz, DMSO) δ 12.76 (s, 1H), 8.22 (d, $J = 7.8$ Hz, 1H), 7.94 (d, $J = 8.7$ Hz, 1H), 7.30–7.17 (m, 10H), 7.15 (td, $J = 5.7, 3.0$ Hz, 1H), 4.55 (ddd, $J = 10.4, 8.6, 4.0$ Hz, 1H), 4.45 (td, $J = 8.2, 5.2$ Hz, 1H), 3.08 (dd, $J = 13.9, 5.2$ Hz, 1H), 3.01–2.89 (m, 2H), 2.68 (dd, $J = 13.9, 10.5$ Hz, 1H), 1.96 (td, $J = 7.3, 2.3$ Hz, 2H), 1.24 (s, 19H), 1.07–0.97 (m, 2H), 0.90–0.80 (m, 4H). ESI-MS calcd m/z 578.4084 [$\text{C}_{36}\text{H}_{54}\text{N}_2\text{O}_4$] $^+$; found 579.4167 [($\text{C}_{36}\text{H}_{54}\text{N}_2\text{O}_4$) + H] $^+$. Elemental analysis for $\text{C}_{36}\text{H}_{54}\text{N}_2\text{O}_4$ calcd: C 74.70%, H 9.40%, N 4.84%; found: C 74.19%, H 9.68%, N 4.61%.

Gel preparation

Fatty acid-peptide conjugates (4 mM) were dissolved in either DMF or DMSO. An equal volume of water was added to the



dissolved peptides, resulting in a final concentration of 2 mM. Solutions were left to rest at room temperature until gelation was visually confirmed with an inverted vial test. Gels will be referred to from here on by conjugate and organic solvent (*i.e.*, **1-DMF**, **2-DMF**, **3-DMF**, **1-DMSO**, **2-DMSO**, **3-DMSO**).

A 4 mM aqueous stock solution of $\text{TbCl}_3 \cdot 6\text{H}_2\text{O}$ was prepared. Tb-peptide hydrogels were formed with the addition and aqueous dilution of the Tb stock solution to the 4 mM dissolved peptides in either DMF or DMSO for a final peptide concentration of 2 mM, the minimum gelation concentration. Tb-peptide gels were formed with a Tb : peptide molar ratio of 1 : 1, 1 : 2, 1 : 3, 1 : 4, and 1 : 5.

Results and discussion

Gelation study

Gelation was triggered through the addition of equal volumes of water to the peptide conjugates (Fig. 1a) dissolved in either DMSO or DMF (Fig. 1b–g). As a result, the organohydrogel hybrids had final concentrations of 2 mM peptide in 1 : 1 DMF/H₂O or DMSO/H₂O. Interestingly, only three out of the six conditions passed the inverted vial test: **2-DMSO**, **3-DMSO**, and **3-DMF** (Fig. 1b, c and e). No gelation of compound **1** was observed under either DMSO/H₂O or DMF/H₂O solvent conditions (Fig. 1a). The failure of compound **1** to gel, despite differing from compound **2** by only four carbon atoms in the fatty acid chain, suggests that its shorter tail lacked the hydrophobic character necessary to promote its self-assembly in aqueous solutions. The reason for **2** being able to self-assemble in DMSO/H₂O but not in DMF/H₂O may be due to the solvent polarities and molecular sizes. As a slightly larger molecule, DMF may interfere with solvent encapsulation. Additionally, its lower polarity and reduced miscibility with water could disrupt hydrogen bonding interactions that are critical for self-assembly and solvent encapsulation. Compound **3** formed a gel in both organic solvents after the addition of water, which is as expected because of its peptide conjugate

bearing the longest fatty acid tail, which contributes to the noncovalent interactions necessary for self-assembly.

Tb³⁺ coordination

Metals such as lanthanides can offer a variety of coordination sites and geometries that may be substantial contributors to self-assembly in terms of molecular recognition.²⁶ The addition of Tb³⁺ resulted in all three peptide conjugates forming gels at a 1 : 1 Tb : peptide ratio for both DMSO/H₂O and DMF/H₂O conditions (Fig. 2a). Under a UV lamp at 254 nm, the resulting Tb : peptide gels also retain the lanthanide's fluorescent properties, resulting in green and blue fluorescent gel materials (Fig. 2b). The slight variation in colour of the fluorescent gel materials may be attributed to the increasing chain lengths from peptides **1** to **3** as the key difference amongst the gels (Fig. 2). The increasing hydrocarbon chains from **1** to **3** result in greater potential van der Waals and hydrophobic interactions amongst the self-assembled and Tb³⁺-complexed peptide conjugates, likely leading to the blue shift in fluorescence from gels of **1** to **3**.²⁷ Tb, however, can coordinate up to nine ligand sites, thus Tb : peptide ratios were investigated from 1 : 1 to 1 : 5 (Fig. S11 and S12). Successful gelation, as per the inverted vial test, was visually confirmed for all ratios for each peptide and solvent condition.

Given Tb's known fluorescent properties as a lanthanide,¹⁷ fluorescence spectra were recorded to examine the peptide coordination behaviour. When excited at 260 nm, new significant peaks are seen with the addition of **1**, **2**, and **3** compared to Tb(m) itself at 489, 546, 584, and 621 nm (Fig. S13–S15). Following the maximum fluorescence peak at 546 nm, the highest fluorescence intensity was found for a 1 : 1 Tb : peptide ratio for peptide conjugates **1–3** (Fig. 3). This suggests preferred coordination of Tb : peptide at a 1 : 1 ratio. Further characterization was thus focused on gels with 1 : 1 Tb : peptide (denoted going forward as **1-TbDMF**, **1-TbDMSO**, *etc.*).

All three peptide conjugates formed gels in both DMSO/H₂O and DMF/H₂O conditions with a 1 : 1 Tb : peptide ratio. However, with up to nine possible ligand sites, questions remain about how the peptide coordinates with Tb and what other species may be occupying the remaining ligand sites. Thus, FT-IR spectroscopy and mass spectrometry were used. The full FT-IR spectra of the peptides and gels can be found in Fig. S16. Potential coordination sites of the diphenylalanine peptide conjugates include the amide backbone and C-terminal

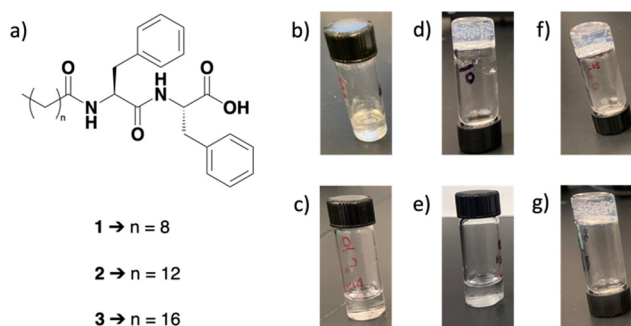


Fig. 1 Structures of fatty acid-conjugated diphenylalanine, specifically caprylated **1**, myristylated **2**, and stearylated **3** diphenylalanine (a), and gelation attempts of 2 mM **1** (b) and (c), **2** (d) and (e), and **3** (f) and (g) in 1/1 DMSO/H₂O (b), (d) and (f) or 1/1 DMF/H₂O (c), (e) and (g). Unsuccessful gels did not pass the inverted vial test: (b) **1-DMSO**, (c) **1-DMF**, (e) **2-DMF**. Successful gels passed the inverted vial test: (d) **2-DMSO**, (f) **3-DMSO**, (g) **3-DMF**.

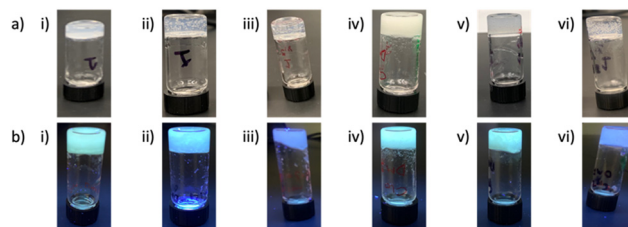


Fig. 2 Successful gel formation under (a) normal light and (b) UV-lamp at 254 nm of: (i) **1-TbDMSO**, (ii) **2-TbDMSO**, (iii) **3-TbDMSO**, (iv) **1-TbDMF**, (v) **2-TbDMF**, and (vi) **3-TbDMF**.



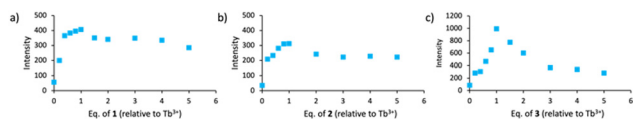


Fig. 3 Fluorescence intensity at 546 nm (ex. 260 nm) for 2 mM of (a) **1**, (b) **2**, and (c) **3** at ratios of 0.2–5 eq. relative to Tb^{3+} in ethanol/water (1:1 v/v).

carboxylate (Fig. 4), the latter of which was reported by Zhou *et al.*²⁴ for xerogels of Fmoc-Phe and Tb^{3+} . A significant peak shift (at least 4 cm^{-1}) in the FT-IR spectra was found in the carboxylate region (1700s cm^{-1})²⁴ for **1-DMF** (1730 cm^{-1}) and **1-DMSO** (1732 cm^{-1}) from **1** (1715 cm^{-1}), **2-DMF** (1728 cm^{-1}) and **2-DMSO** (1711 cm^{-1}) from **2** (1717 cm^{-1}), and **3-DMF** (1730 cm^{-1}) from **3** (1715 cm^{-1}). In the amide I region (1600s cm^{-1}),^{28,29} significant peak shifts were found for **1-DMF** (1651 cm^{-1}) and **1-DMSO** (1632 cm^{-1}) from **1** (1628 cm^{-1}), and **2-DMSO** (1639 cm^{-1}) from **2** (1643 cm^{-1}). In the amide II region (1500s cm^{-1}),²⁹ a significant peak shift was found only for **1-DMF** and **1-DMSO** (1560 cm^{-1}) from **1** (1556 cm^{-1}), and **3-DMSO** (1539 cm^{-1}) from **3** (1543 cm^{-1}). It is most likely that the C-terminal carboxylate participates in Tb coordination, with potential involvement of the amide backbone. Additional regions of interest also included the hydrogen region, 3000–4000 cm^{-1} , wherein the C-terminal carboxylic –OH stretch and the amide –NH stretch may be found. Given the significant peak shifts discussed above, pointing towards the involvement of the carboxylate and the amide backbone, analysis of the higher wavenumber region was also initially expected to provide some insights. The peak found in this region is likely the –NH stretching²⁴ as the peptides gelled in water would be fully deprotonated at the C-terminal. Although we did not find significant peak shifts, the increased peak broadening of the xerogel peaks in this region (Fig. S16) can be attributed to hydrogen bonding in the self-assembled metal-peptide gels²⁴ and possibly solvent (*i.e.*, water) molecules participating in the coordinated complexes. Thus, other analytical methods were also used.

X-ray diffraction (XRD) studies can be used for the investigation of samples' physical properties, most commonly for crystalline materials and structures, along with sample compositions. Crystals, as a highly ordered and thermodynamically stable solid state, typically yield sharp peaks in their diffraction profiles that clearly distinguish samples from amorphous materials that yield plateaus,

undefined and/or exceedingly broad peaks.³⁰ In the case of gels, where the metastable supramolecular network immobilizes the fluid, XRD studies can provide diffraction profiles that give some insight into the assembly structure of the sampled material. For peptide gels, the molecular packing of the self-assembled gelators can be characterized, as reported by Nanda *et al.*,³¹ with aromatic–aromatic interactions from a peak at $2\theta = 23.4^\circ$, where π – π stacking distance was demonstrated by a d value of 3.7 Å. They also reported the antiparallel β -sheet structure of their Boc-Phe-Phe-Ala-OH hydrogel, determined by peaks at $2\theta = 8.4^\circ$ and 18.15° with d spacing of 10.53 Å and 4.88 Å, respectively. In xerogels of **1-TbDMF** and **1-TbDMSO** (Fig. S17), peaks were found for $2\theta = 14.80^\circ$, 19.14° , 36.31° and 14.82° , 19.12° , 36.67° . These three broad peaks suggest non-crystallinity, which is expected for these soft gel materials, along with some physical ordering (*i.e.*, the organohydrogels are not completely amorphous solids), giving rise to d values of about 2.75 Å at $\sim 15^\circ$ and 2.13 Å at $\sim 19^\circ$. The XRD profiles across all other samples were analogous and not included. Although this does not exactly match the π – π stacking distance, as reported by Nanda *et al.*,³¹ this may be due to the increased disorder and assembly variability triggered by the nine potential ligand sites of Tb.

To investigate the potential complexes and coordinated species occupying the Tb-ligand sites, mass spectrometry was used on all six lyophilized gels. Potential complexes were screened based on one peptide (**1–3**) and one Tb, along with up to eight solvent molecules of either H_2O , DMSO/DMF, or a combination of DMSO/ H_2O or DMF/ H_2O for a total of nine potential ligands as Tb(III) has been reported with up to nine coordinated species.^{32,33} Through electrospray ionization, a variety of coordinated species were found (Table 1). Spectra of all found species for each gel can be found in Fig. S5–S10. Water is found to coordinate in all six gels at up to eight H_2O . Coordination to just the organic solvent DMSO or DMF as well as a combination of organic solvent and H_2O is also found for **1-DMF**, **2-DMF**, **2-DMSO**, and **3-DMSO**. Only one H_2O coordinated **1-Tb** was found in **1-DMSO** and **3-Tb** in **3-DMF**. We would expect, given that the only differing factor among peptide conjugates **1–3** is the length of the fatty acid tail, that the

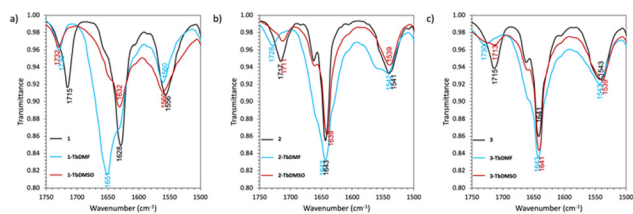


Fig. 4 FT-IR spectra of the carboxylate (1700s cm^{-1}), amide I (1600s cm^{-1}), and amide II (1500s cm^{-1}) regions of (a) **1**, **1-TbDMF**, **1-TbDMSO**, (b) **2**, **2-TbDMF**, **2-TbDMSO**, and (c) **3**, **3-TbDMF**, **3-TbDMSO**. Peptides **1–3** are depicted in black, DMF/ H_2O gels in blue, and DMSO/ H_2O gels in red.

Table 1 Solvent-coordinated species of H_2O , organic (DMF/DMSO), or a combination of both found in 1:1 Tb:peptide gels through mass spectrometry

Gel	Solvent	Solvent-coordinated species														
1-TbDMF	H ₂ O	0	1	4	8	0	0	0	0	1	4	5	6	7		
	DMF	0	0	0	0	1	4	7	8	7	4	3	2	1		
1-TbDMSO	H ₂ O	0	1													
	DMSO	0	0													
2-TbDMF	H ₂ O	0	1	5	8	0	0	6	7							
	DMF	0	0	0	0	1	5	2	1							
2-TbDMSO	H ₂ O	0	1	2	3	4	7	8	0	0	0	0	2	3	4	5
	DMSO	0	0	0	0	0	0	0	1	4	6	7	6	5	4	3
3-TbDMF	H ₂ O	0	1													
	DMF	0	0													
3-TbDMSO	H ₂ O	0	1	3	4	0	0	3	7							
	DMSO	0	0	0	0	1	3	5	1							



coordinated species would all be the same and consistent within solvent conditions or between peptides. However, this is not the case. The variance of coordinated species found through mass spectrometry between the peptides and solvent conditions could be attributed to the ionization process and complex stability. There may be more coordinated species present that did not survive ionization to be detected; however, we demonstrate the variability in Tb(III) coordination in these gelling conditions with peptide conjugates 1–3.

Tb³⁺ gel characterization

The morphologies of the organohydrogel hybrids were examined through SEM imaging of the lyophilized gels (Fig. 5) along with TEM imaging of the nanostructures (Fig. 6). There is a visible difference among the DMSO/H₂O and DMF/H₂O gels, as well as among 1–3, through SEM characterization of the material morphologies. 1-DMSO and 1-DMF (Fig. 5a and b) are fairly structurally similar, with small pores in their 3-dimensional self-assembled structures. 2-DMSO (Fig. 5c) has a more porous structure than 1-DMSO and 1-DMF with visible sheets connecting the structures, whereas 2-DMF (Fig. 5d) has clear twisted fibrillar structures. 3-DMSO (Fig. 5e) is similar to 2-DMSO in the sheet-like structures but does not show the same porosity that is found in 3-DMF (Fig. 5f).

TEM imaging of the self-assembled nanostructures is limited, however, in its representation of a very thin, minimal sample of the gels. Although at higher resolution, the images are not as representative of the 3-dimensional structural morphologies as SEM imaging, which also provides insight towards the nanostructures leading to supramolecular gel formation. Entangled microscale fibrous networks (Fig. 6a–c and e–f), along with tape-like structures (Fig. 6d) can be seen in SEM imaging. Although at a lower magnification than TEM imaging, and despite imaging of lyophilized gel samples, SEM can give greater insight to the morphologies responsible for supramolecular gelation. At the nanoscale, as seen through TEM, nanofibrous networks prevail. At the microscale, as seen through SEM, much larger structures are observed that likely arose from the dense conglomeration of the nanofibrous networks. Overall, electron microscopy characterization of the morphologies highlights the impact that a difference of just four carbon atoms, and a choice of solvent, can have on

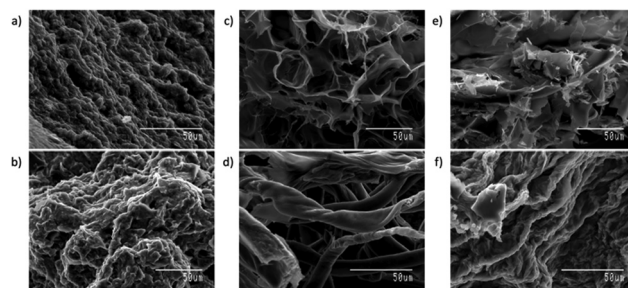


Fig. 6 SEM imaging of lyophilized gel morphologies of (a) 1-TbDMSO, (b) 1-TbDMF, (c) 2-TbDMSO, (d) 2-TbDMF, (e) 3-TbDMSO, and (f) 3-TbDMF. Scale bar 50 μ m.

gelators during the spontaneous self-assembly process into higher-order structures.

To examine the viscoelastic properties of these materials, rheological studies were performed. The formation of a gel state is reinforced from the inverted vial tests (Fig. 2a) through frequency sweeps demonstrating the storage modulus G' being greater than the loss modulus G'' (Fig. 7). Considering that self-assembly of these physical gels is contingent on noncovalent interactions, we would expect that a higher number of possible noncovalent interaction sites would result in a stronger gel material. Overall, gels of 3 were predicted to have higher G' values, followed by gels of 2, then 1 from longest to shortest acyl chain lengths and thus greatest to least possible potential noncovalent interactions. Instead, we found a notable decrease in G' for 3-DMSO and 3-DMF (Fig. 7e and f) compared to Tb-peptide gels of 1 (Fig. 7a and b) and 2 (Fig. 7c and d) of the corresponding solvent conditions. G' for 1-DMF and 2-DMF (Fig. 7b and d) were relatively similar, whereas there was a slight increase in G' from 1-DMSO to 2-DMSO (Fig. 7a and c). Amplitude sweeps (Fig. 8) were used to examine the mechanical behaviour of the soft materials under increasing strain. The results showed that 1-TbDMSO and 2-TbDMSO had comparable gel-sol transitions at around 15% strain, whereas 3-TbDMSO transitioned at around 30% strain. Under mechanical disruption, this demonstrates that the longer acyl chain gelator yielded a more robust self-assembled material, potentially due to increased noncovalent interactions present in the kinetically trapped nanostructures. Additionally, although there is a clear structural morphology change in the Tb-peptide gels

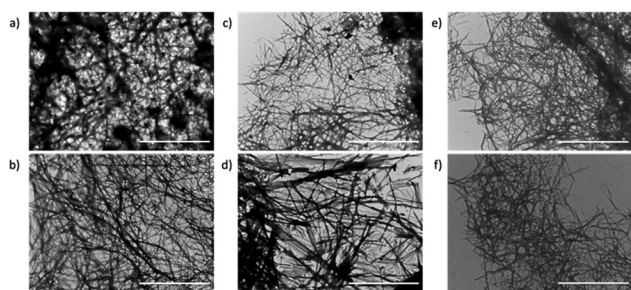


Fig. 5 TEM imaging of the gel morphologies of (a) 1-TbDMSO, (b) 1-TbDMF, (c) 2-TbDMSO, (d) 2-TbDMF, (e) 3-TbDMSO, and (f) 3-TbDMF. Scale bar: 10 μ m.

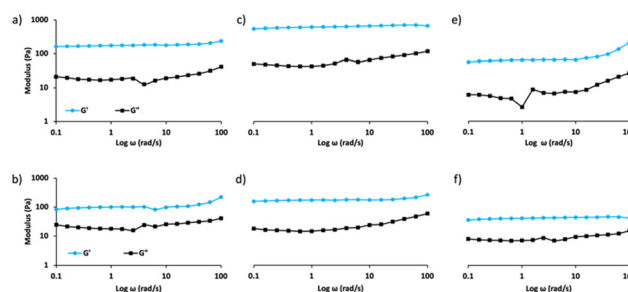


Fig. 7 Frequency sweeps from 0.1 to 100 rad s^{-1} for (a) 1-TbDMSO, (b) 1-TbDMF, (c) 2-TbDMSO, (d) 2-TbDMF, (e) 3-TbDMSO, and (f) 3-TbDMF.



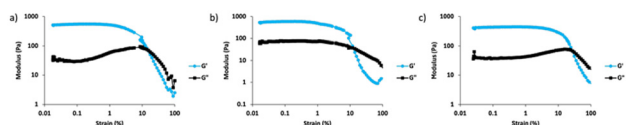


Fig. 8 Amplitude sweeps from 0.01 to 100% strain for (a) **1-TbDMSO**, (b) **2-TbDMSO**, and (c) **3-TbDMSO** at 10 rad s^{-1} .

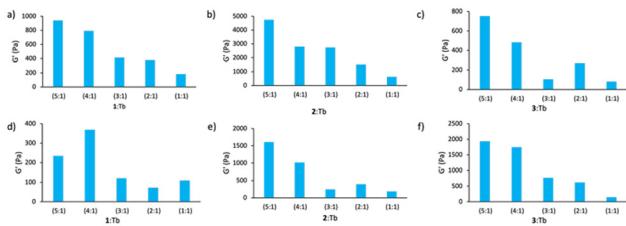


Fig. 9 Histograms comparing average G' at varying peptide:Tb ratios in (a)–(c) DMSO/ H_2O and (d)–(f) DMF/ H_2O .

formed from **1** to **2** to **3**, as seen in SEM (Fig. 5), there is not much correlation of those structural changes to the mechanical strengths of these viscoelastic materials (Fig. 7). Overall, the most ordered structural morphologies of **2** (Fig. 5c and d) also appear to have the generally highest mechanical strengths (Fig. 7c and d), which may indicate that a C_{14} -length fatty acid tail is optimal for the self-assembly of higher-ordered nanostructures and resulting material strength. Further modulation of the gel material can be done through increasing the peptide-to- Tb^{3+} ratio, which resulted in successful gelation as stated earlier. Increasing the concentration of peptide gelator in almost all gel cases for **1**–**3** in DMSO/ H_2O or DMF/ H_2O showed a general trend of increasing storage modulus (Fig. S18–S23). An overall histogram comparison of the average G' values (Fig. 9) in most cases demonstrates the expected general trend of lower gelator concentration yielding lower material strength. However, this trend is not exactly linear across all variations. Further studies must be done to determine the specific tunability of this series of soft, peptide-based materials. However, two preliminary variable pathways have been demonstrated by the addition of Tb^{3+} , as well as by varying the peptide to Tb^{3+} ratio, to pursue fluorescence and to access different viscoelastic or nanostructural properties.

Conclusions

Lanthanides are an interesting category of metallic stimuli for self-assembly and gel formation as they can impart photoluminescent properties and have numerous coordination chemistries and geometries. The nine possible ligand sites of Tb used in this study helped to highlight the variability present in metastable physical gels, as we have demonstrated the variety of solvent ligands based on a fluorescence-determined 1:1 Tb^{3+} :*N*-acylated diphenylalanine ratio in a series of organohydrogel hybrid materials. We also report a surprising optimum carbon chain length of 14 as C_{14} -FF-OH hybrid gels resulted in the highest average elastic moduli with porous self-assembled

network structures over the C_{10} -FF-OH and C_{18} -FF-OH counterparts, although C_{18} -FF-OH withstood a high strain-induced gel-sol transition. With our *N*-acylated diphenylalanine conjugates, we have shown that the addition of Tb^{3+} was able to act as a stimulus to trigger gelation in those that did not gel with simply the addition of water to the organic-dissolved peptides. Overall, self-assembly is shown to be a spontaneous process and is often unpredictable, with each variable yielding significant variation in the properties of the resulting soft materials. We anticipate that this work opens a new avenue for lanthanide-gel materials to involve peptide-based design and believe that this further reinforces the versatility of the diphenylalanine motif in gel materials and the need for greater elucidation of self-assembly pathways to target tunable properties.

Conflicts of interest

There are no conflicts to declare.

Data availability

The data supporting this article have been included as part of the SI.

Additional spectroscopic characterization of peptides **1** and **3** along with spectroscopic and rheological characterization of Tb-peptide gels. See DOI: <https://doi.org/10.1039/d5nj02838h>

Acknowledgements

We would like to thank and acknowledge the financial support received from the University of Toronto and Natural Sciences and Engineering Research Council (RGPIN-2022-03129). We would also like to thank and acknowledge Bruno Chue and Durga Acharya from the Centre for the Neurobiology of Stress (CNS) at the University of Toronto Scarborough for their help in microscopy imaging. We acknowledge that this is possible due to the CFI grant (#493864) that established the CNS Core Facility. We would also like to thank and acknowledge Tony Adamo from the TRACES Centre at the University of Toronto Scarborough and the ANALEST Facility at the University of Toronto St. George for their instrumental help in characterization. We would also like to acknowledge and thank Ahmer Imam and the Voznyy lab at the University of Toronto Scarborough for their help in XRD measurements. We would also like to acknowledge the use of BioRender.com (2023) in the creation of figures and schemes.

Notes and references

- 1 T. Christoff-Tempesta, A. J. Lew and J. H. Ortony, *Gels*, 2018, 4(2), 40.
- 2 J. F. Douglas, *Gels*, 2018, 4(1), 19.
- 3 P. R. A. Chivers and D. K. Smith, *Nat. Rev. Mater.*, 2019, 4, 463–478.



- 4 S. Maeda, Y. Hara, S. Nakamaru and S. Hashimoto, *Polymers*, 2011, **3**(1), 299–313.
- 5 N. A. Peppas and Y. Huang, *Pharm. Res.*, 2002, **19**, 578–587.
- 6 F. Liu and M. W. Urban, *Prog. Polym. Sci.*, 2010, **35**(1–2), 3–23.
- 7 Abdullah, L. Liu and H. Umer Javed, *J. Xiao. Front. Nutr.*, 2022, **9**, 890188.
- 8 G. Rando, S. Sfameni and M. R. Plutino., *Gels*, 2023, **9**(1), 9.
- 9 M. Caldeira Barbosa, G. Leite Silva, E. B. Macedo Viana, R. C. Ferreira Bonomo, L. Brito Rodrigues and C. Martins Veloso, *J. Food Sci. Technol.*, 2023, **60**(12), 2916–2926.
- 10 B. Pramanik and S. Ahmed, *Gels*, 2022, **8**(9), 533.
- 11 M. Kurbasic, E. Parisi, A. M. Garcia and S. Marchesan, *Curr. Top. Med. Chem.*, 2020, **20**(14), 1300–1309.
- 12 S. Mondal, S. Das and A. K. Nandi, *Soft Matter*, 2020, **16**(6), 1404–1454.
- 13 T.-T. Lu, J. Liu, H. Li, T.-B. Wei, Y.-M. Zhang and Q. Lin, *Prog. Chem.*, 2016, **28**(10), 1541–1549.
- 14 J. Mayr, C. Saldias and D. D. Diaz, *Chem. Soc. Rev.*, 2018, **47**(4), 1484–1515.
- 15 J. Zhang and C.-Y. Su, *Coord. Chem. Rev.*, 2013, **257**(7–8), 1373–1408.
- 16 G. Picci, C. Caltagirone, A. Garau, V. Lippolis, J. Milia and J. W. Steed, *Coord. Chem. Rev.*, 2023, **492**, 215225.
- 17 M. Elbanowski and B. Makowska, *J. Photochem. Photobiol., A.*, 1996, **99**(2–3), 85–92.
- 18 M. He, L. Wang, J. Wu and J. Xiao, *Chem. Eur. J.*, 2016, **22**(6), 1914–1917.
- 19 X. Chen, Y. Wang, R. Chai, Y. Xu, H. Li and B. Liu, *ACS Appl. Mater. Interfaces*, 2017, **9**(15), 13554–13563.
- 20 D. Gu, W. Yang, D. Lin, X. Qin, Y. Yang, F. Wang, Q. Pan and Z. Su, *J. Mater. Chem. C*, 2020, **8**(39), 13648–13654.
- 21 B. Li, Z. Song, K. Zhu, Q. Niu, Z. Li and H. Li, *ACS Appl. Mater. Interfaces*, 2021, **13**(17), 20633–20640.
- 22 N. Falcone, N. M. O. Andoy, R. M. A. Sullan and H.-B. Kraatz, *ACS Appl. Bio Mater*, 2021, **4**(9), 6652–6657.
- 23 N. Falcone, T. Shao, N. M. O. Andoy, R. M. A. Sullan, X. Sun and H.-B. Kraatz, *Biomater. Sci.*, 2020, **8**(20), 5601–5614.
- 24 Q. Zhou, X. Dong, J. Yuan, B. Zhang, S. Lu, Y. Xiong, Y. Liao, Q. Wang, Y. Yang and H. Wang, *J. Mol. Liq.*, 2019, **292**, 111373.
- 25 S. Yang, X. R. Pan, J. P. Tang, C. Yao and D. Y. Yang, *Sci. China: Technol. Sci.*, 2022, **65**, 1043–1051.
- 26 G. Moreno-Alcántar, *Eur. J. Inorg. Chem.*, 2023, (16), e202200788.
- 27 F. H. dos Santos Rodrigues, G. Garcia Delgado, T. Santana da Costa and L. Tasic, *BBA Adv*, 2023, **3**, 100091.
- 28 I. Marcotte, A. Bélanger and M. Auger, *Chem. Phys. Lipids*, 2006, **139**(2), 137–149.
- 29 S.-Y. Lin, H.-L. Chu and Y.-S. Wei, *J. Biomol. Struct. Dyn.*, 2003, **20**(4), 595–601.
- 30 R. Ricciardi, F. Auriemma, C. De Rosa and F. Lauprêtre, *Macromolecules*, 2004, **37**(5), 1921–1927.
- 31 J. Nanda, B. Adhikari, S. Basak and A. Banerjee, *J. Phys. Chem. B*, 2012, **116**(40), 12235–12244.
- 32 J. Ran, X. Zhao, X. Hu, Y. Chen and Z. Tian, *Polyhedron*, 2021, **194**, 114910.
- 33 H. Wang, L. Niu, G. Li, W. Zhang and X. Chen, *J. Mol. Struct.*, 2020, **1211**, 128081.

